NOVEL EMITTANCE DIAGNOSTICS FOR DIFFRACTION LIMITED LIGHT SOURCES BASED ON X-RAY FRESNEL DIFFRACTOMETRY

M. Masaki#, Y. Shimosaki, S. Takano, M. Takao
Japan Synchrotron Radiation Research Institute (JASRI/SPring-8), Hyogo, Japan

Abstract

A novel emittance diagnostics technique with high sensitivity using X-ray Fresnel diffraction by a single slit has been developed to measure micron-order electron beam sizes at insertion devices (IDs) of photon beamlines. The X-ray Fresnel diffractometry (XFD) is promising for diagnostics especially of a so-called diffraction limited storage ring with ultra-low emittance. The XFD observes a double-lobed diffraction pattern that emerges by optimizing the single slit width. The principle is based on a correlation between the depth of a median dip in the double-lobed pattern and the light source size at the ID. The validity of the new technique was theoretically and experimentally studied. The achievable resolution of the XFD will be also discussed.

INTRODUCTION

In recent years, a diffraction limited storage ring (DLSR) [1] as ring-based future light sources has been extensively and intensively discussed, aiming to drastically boost the average brilliance and the transverse coherence by orders of magnitude compared with existing storage rings. In the DLSR, due to inevitable field errors of strong quadrupole and sextupole magnets, unwanted distortion of lattice functions and local betatron coupling may result in a different light source size at each X-ray photon beamline. One of the most important things for synchrotron light sources is to maximize the light performance at photon beamlines for user experiments. Therefore, measurements of electron beam sizes at the ID source points will be more crucial for securing the absence of degradation of brilliance and transverse coherence of radiation at the beamlines. So far, various techniques have been developed to measure the micron-order vertical beam sizes, for examples, π-polarization imaging method [2], method using a vertical undulator spectra [3], widely used X-ray pinhole cameras (XPCs) e.g. [4], an X-ray imaging method using Fresnel zone plates [5][6] and interferometric techniques [7][8]. However, these methods are not necessarily as readily applicable as they are to emittance diagnostics of all the ID sources of the beamlines. Therefore, development of a new emittance diagnostics technique universally applicable to all the ID beamlines is necessary. We have developed a novel emittance diagnostic method, X-ray Fresnel diffractometry (XFD) [9]. It is capable of resolving a micron-order beam size at the ID source point with high sensitivity and available at typical photon beamlines equipped with a 4-jaw slit and a monochromator.

masaki@spring8.or.jp

PRINCIPLE OF XFD

The XFD observes a double-lobed diffraction pattern that emerges by optimizing a single slit width A under given conditions of distance L from a source point to the slit, distance R from the slit to an observation point, and the observing wavelength λ (Fig. 1). The principle of XFD is based on the correlation between the depth of the median dip in the double-lobed pattern and the light source size; i.e., the dip becomes shallow with growth in the source size. The only requirement for light sources is that the radiation should be a spherical wave with a flux distribution wider than the slit width. Therefore, the XFD is applicable to both most types of ID sources and bending magnet sources.

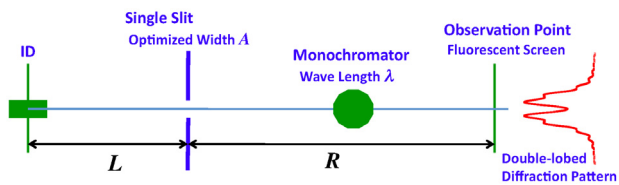

Figure 1: Layout of ID source size measurement using the XFD.

In a one-dimensional case for simplification, a point spread function (PSF) at the observation point is expressed by the following Fresnel integral,

$$I(y,y_e) \propto \left| \int_{-A/2}^{A/2} \sqrt{I_s(y_s - y_e)} \exp\left[i \frac{\pi}{\lambda} \left\{ \frac{1}{L} + \frac{1}{R} \right\} \left\{ (y_s - y_e) - \frac{L(y - y_e)}{L+R} \right\}^2 \right] dy_s \right|^2 \quad (1)$$

where the function $I_s(y_s\text{-}y_e)$ is the radiation flux distribution at the slit, y_e, y_s and y are an electron position at source point, coordinates on the slit and the screen, respectively. An optimized slit width to obtain the double-lobed diffraction pattern is given by a following formula derived from a destructive interference condition of the light at the center (y=0),

$$A \approx \sqrt{7\lambda \frac{LR}{L+R}}. \quad (2)$$

The distance between two lobe peaks, i.e., the pitch P, is expressed as follows from a constructive interference condition of the light,

ISBN 978-3-95450-141-0

$$P = 2\lambda\frac{R}{A} = 2\sqrt{\frac{\lambda}{7}\frac{R(L+R)}{L}}. \quad (3)$$

The PSF of Eq. (1) is shifted by $-(R/L)y_e$ depending on the electron position y_e at the source point. This shift creates sensitivity to changes in the electron beam size. While, the small electron orbit angle y'_e at the source point has little effect on the PSF, because a spherical phase distribution of the radiation on the slit is independent of the orbit angle. Therefore, an electron beam angular divergence, if it is smaller than 10 μrad (r.m.s.), has little influence on the observed diffraction patterns.

The XFD scheme needs the monochromatic X-ray. According to a numerical analysis, the peak-to-peak photon bandwidth narrower than $\Delta\lambda/\lambda \sim 2\%$ is necessary to be negligible distortion of the PSF with the finite bandwidth. A widely-used silicon (111) as a monochromator crystal generates an X-ray beam with the photon bandwidth of 10^{-4} sufficiently narrower than 2%.

The undulator and wiggler radiations have light properties required by XFD. The wavefront is well-approximated by a spherical wave with a parabolic phase distribution around a longitudinal light axis. Furthermore, the flux of the on-axis resonant wavelength has an intensity distribution with a flat top wider than the slit width of several tens of microns [10].

SIMULATION FOR SOURCE SIZE MEASUREMENT AT DLSR

The source size measurement using the XFD at a DLSR photon beamline has been simulated. We assumed a distance of L = 25 m from source to slit, R = 25 m from slit to observation screen, and an X-ray energy of 40 keV. The double-lobed diffraction pattern with the deepest dip is formed when the slit width is 52 μm from Eq. (2). Figure 2 shows the calculated PSF assuming a constant $I_s(y_s\text{-}y_e)$ and its convolution with Gaussian-distributed sources. The peak-to-valley intensity ratio I_v/I_p of the median dip has a high sensitivity to micron-order changes in the root mean square (r.m.s.) source size of less than 10 μm, corresponding to vertical electron beam sizes at the ID source points, where a vertical emittance from 10 to 20 pm.rad and a vertical betatron function of several meters are assumed. In Fig. 3, the peak-to-valley ratios I_v/I_p as a function of the source size are shown as sensitivity curves for three different X-ray energies of 40, 16, and 7.2 keV, where the slit width is optimized for each X-ray energy. The observing X-ray energy can be tuned by a beamline monochromator depending on the range of measuring source sizes. The XFD using photon energy of 7.2 keV is also applicable to the measurement of horizontal source sizes of about 20 μm corresponding to an ultra-low horizontal emittance of about 100 pm.rad of DLSR.

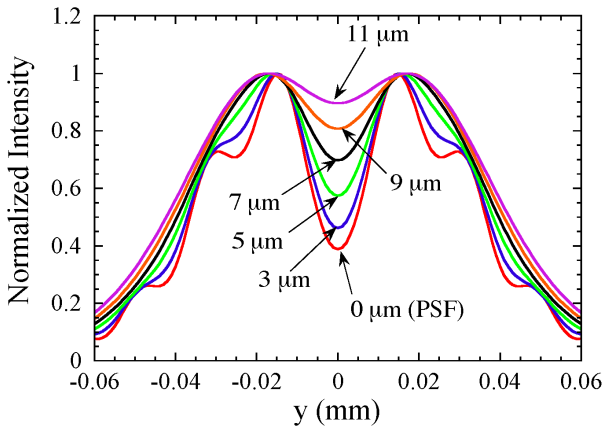

Figure 2: The calculated PSF and its convolution with Gaussian-distributed sources having sizes from 3 to 11 μm (r.m.s.), assuming X-ray energy of 40 keV, distances of 25 m from source to slit and slit to observation screen.

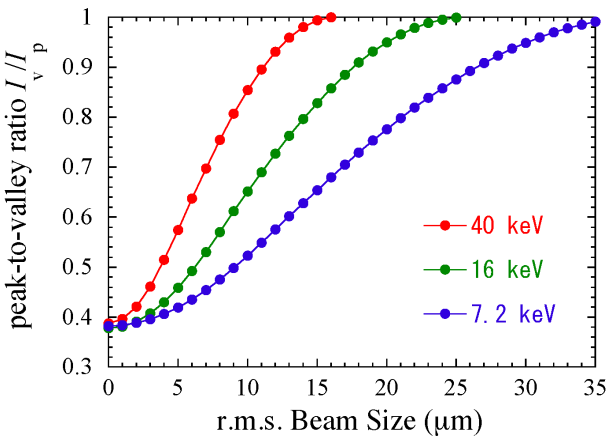

Figure 3: Calculated sensitivity curves at some X-ray energies. Red, green and blue dots show the curves at 40, 16 and 7.2 keV, respectively.

EXPERIMENTAL STUDY AT SPRING-8

We have confirmed XFD's sensitivity to changes in the source sizes experimentally by observing the double-lobed Fresnel diffraction patterns for some different vertical beam emittances at an ID source point. The measurements were performed at the SPring-8 diagnostics beamline (BL05SS) [10] with a planar undulator (ID05) [11]. The beamline front-end slit is located at a distance of 26.8 m from the source point, and 65.4 m from the slit to the observation position. The double-lobed patterns were observed by a high-resolution X-ray imaging system (HAMAMATSU), which consists of a P43 fluorescent screen, an imaging optics with lenses, and a CCD camera. The resolution of the imaging system was calibrated by sharpness of observed edge a stainless steel wire of 0.5 mm diameter placed in front of the system. The result was 6.8 μm (r.m.s.) in scale at the

ISBN 978-3-95450-141-0

ID05 source point. The measuring integration time was set at a minimum of 1 ms to reduce the influence of the vibration of the cryogenically cooled monochromator crystals. An X-ray energy of 7.2 keV for the fundamental harmonic radiation with a deflection parameter K = 0.46 was selected by the monochromator. The X-ray energy was fine-tuned to 7.167 keV in the range of the spectrum band of the harmonic radiation to maximize the vertical flat top width of an observed flux distribution with the fully opened front-end slit. From Eq. (2), the optimized vertical slit width is 150 μm, which was consistent with the experimentally adjusted width to provide the deepest median dip in the observed double-lobed pattern. A narrow horizontal slit of 200 μm was also empirically adjusted to provide the deepest dip as well as the vertical slit. Figure 4 shows four examples of Fresnel diffraction images observed at different operation points of the storage ring by moving horizontal betatron tunes, both with and without the skew quadrupole magnetic fields for XY betatron coupling correction. The double-lobed structures are clearly observed in the vertical direction; however, in the horizontal direction, the diffraction patterns are smeared out due to the large horizontal emittance. The vertical line-projected profiles of the four 2D images are shown in Fig. 5.

To evaluate the vertical beam sizes at ID05 from the observed double-lobed patterns, the PSF of this experimental setup is needed. In a strict calculation of the PSF, the vertical flux distribution $I_s(y_s\text{-}y_e)$ given in Eq. (1) needs to include contributions of off-axis and off-resonant radiations coming from the horizontal emittance and the energy spread of electron beam, respectively. The flux distribution calculated at 7.167 keV assuming a single electron of zero horizontal emittance and zero energy spread does not include those contributions. However, since a rigorous treatment of the effects of the horizontal emittance and the energy spread requires very elaborate computation, we assumed the measured flux distribution at 7.167 keV with a fully opened vertical slit as $I_s(y_s\text{-}y_e)$. The experimental flux distribution effectively includes the contributions of the off-axis and off-resonant radiations. Using the PSF based on the measured flux distribution, the vertical beam sizes were evaluated by fitting Gaussian source convolved with the PSF to the experimental line-projected profiles. The fitted function $f(y)$ is expressed as,

$$f(y) = C\int_{-\infty}^{\infty} I(y,y_e)\exp\left[-\frac{(y_e - y_0)^2}{2(\sigma_{y,e}^2 + \sigma_{res}^2)}\right]dy_e, \quad (4)$$

where the fitting free parameters are a normalization factor C, a center position y_0, a vertical electron beam size $\sigma_{y,e}$ at a source point. The parameter σ_{res} is the imaging system resolution of 6.8 μm (r.m.s.) mentioned above. The smallest in the evaluated beam sizes is 8.1 μm (r.m.s.) for the red profile with the deepest dip in Fig. 5. To analyze the red data, a comparison between the experimental profile and calculated profiles for some beam sizes deviating from the best-fitted size of 8.1 μm is shown in Fig. 6. The function, Eq. (4) with beam size deviations of 0.5 μm step is calculated. The deviation of at least 0.5 μm looks distinguishable from the best-fitted curve. We conclude that light source size smaller than 10 μm (r.m.s.) was successfully resolved, and the resolution was in the order of sub-micron (~0.5 μm).

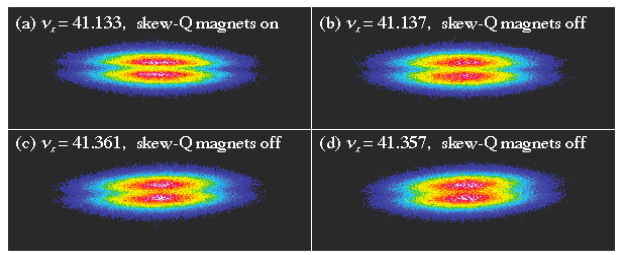

Figure 4: Double-lobed diffraction images observed at four different vertical emittances, changing operation points with different horizontal betatron tunes ν_x, turning skew quadrupole magnets on and off.

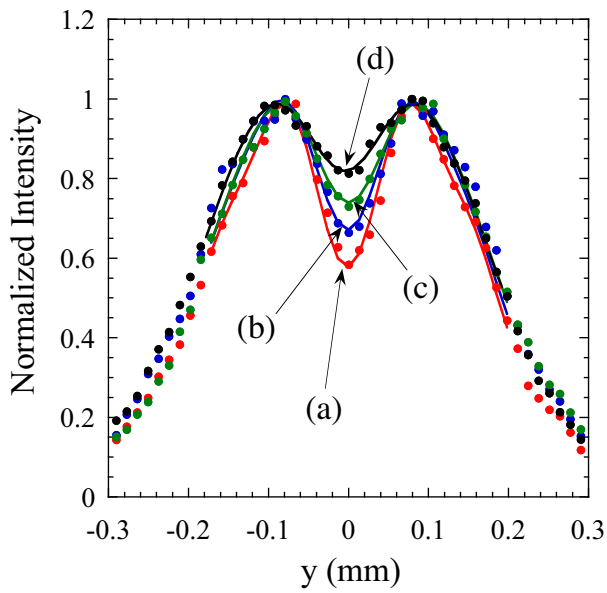

Figure 5: Normalized vertical line-projected profiles (dots) of the four 2D images, their fitted curves (solid lines) by Gaussian source distributions convolved with the PSF. Red, blue, green, and black correspond to (a), (b), (c) and (d) in Fig. 4, respectively.

We also simultaneously measured vertical beam sizes at two separate bending magnet sources using the X-ray beam imager (XBI) [6] by a Fresnel zone plate and the 2D-interferometer [8] by a diffraction mask with four circular apertures instead of a double slit. Figure 7 shows the comparison between three measurements using XFD, XBI and 2D-interferometer, where the beam sizes are

ISBN 978-3-95450-141-0

normalized by the square root of the vertical betatron functions at each source point. The black solid line in Fig. 7 shows the case where the global betatron coupling model is a good approximation, viz. the XY emittance coupling ratio is independent of the position along the storage ring. The correlation between three measurements has a trend along the black linear line. However the scatters of data around the black line are larger than the error bars. We deduce the scatters to be an influence of the local betatron coupling resulting in position-dependent XY emittance coupling ratio along the ring.

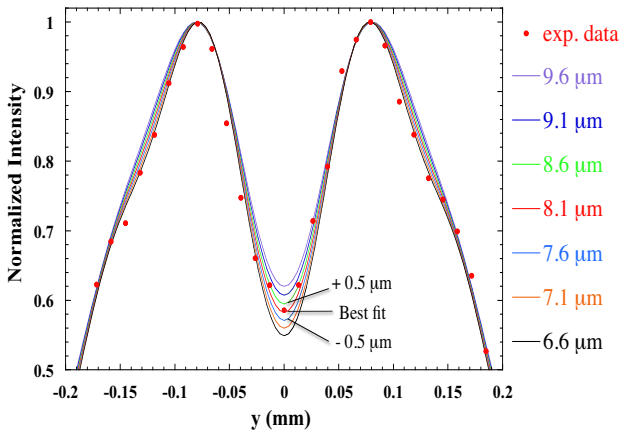

Figure 6: Comparison between the experimental data with the deepest dip and calculations for beam sizes deviating from the best-fitted size of 8.1 μm. The deviations are 0.5 μm step.

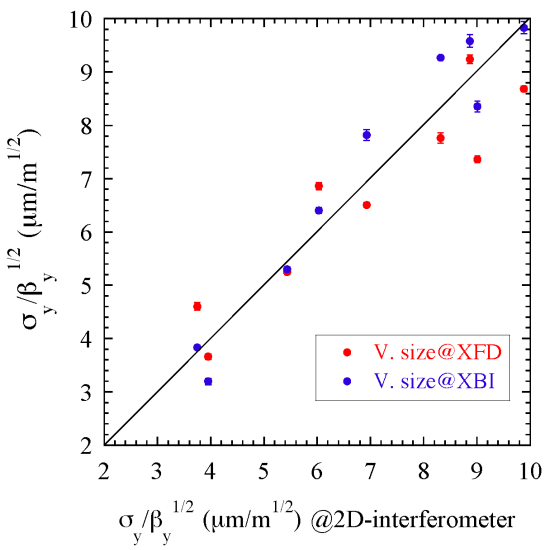

Figure 7: Comparison between results of the simultaneous measurements by XFD at the ID05 source, X-ray beam imager (XBI) and 2D-interferometer at two separate bending magnet sources. The X-axis is the result of 2D-interferometer. On the Y-axis, Red and blue dots indicate the results by XFD and XBI, respectively. The black line shows a correlation on the global betatron coupling model.

TWO-DIMENSIONAL MEASUREMENT FOR FUTURE LIGHT SOURCES

The XFD technique, obviously, can be expanded to two-dimensional measurement. We simulated a two-dimensional scheme with the capability of simultaneous measurement of the horizontal and vertical beam sizes. Assuming a 150 μm square slit, distances 26.8 m from source to slit, 65.4 m from slit to observation screen and X-ray energy of 7.2 keV, a calculated 2D point spread function is shown in Fig. 8. As an example for finite source size, Figure 9 shows a diffraction pattern convoluted by the 2D Gaussian source with the horizontal and vertical sizes of 20 μm (r.m.s.) and 10 μm (r.m.s.), respectively. From cross sections of this 2D pattern, we can obtain the double-lobed profiles in the horizontal and vertical directions, independently. Especially for future light sources such as diffraction limited light sources with ultra-low emittance, the horizontal emittance is expected to be small, comparable to the vertical emittance. For such a case, this two-dimensional scheme will be effective.

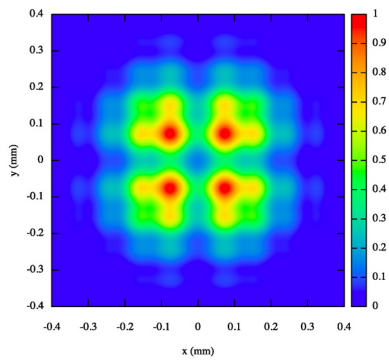

Figure 8: 2D point spread function by assuming a 150 μm square slit, X-ray energy of 7.2 keV and the distances 26.8 m from source to slit, 65.4 m from slit to observation point.

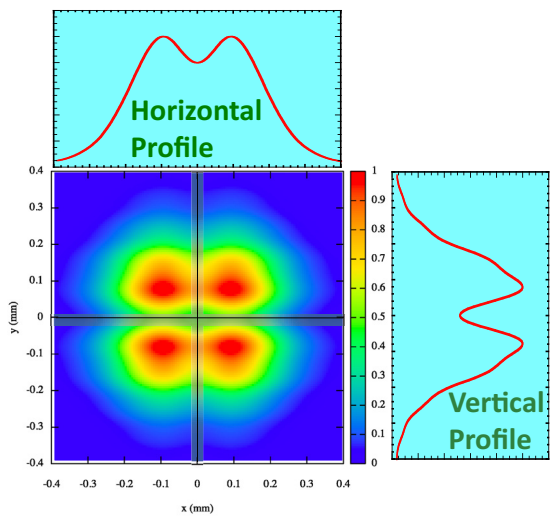

Figure 9: A 2D pattern convoluted by Gaussian source distribution with the horizontal and vertical sizes of 20 μm (r.m.s.) and 10 μm (r.m.s.), respectively.

ISBN 978-3-95450-141-0

ACHEIVABLE RESOLUTION OF XFD

We discuss the achievable resolution of XFD, and compare it with a widely-used and conventional X-ray pinhole camera (XPC). For both cases, a straightforward way to improve the resolution is to place the slit or pinhole close to the source point. For example, we assume that the slit (pinhole) can be placed at a distance of 3 m for both cases, and the observation point is to be 9m from the slit (pinhole), and X-ray energy is 40 keV. In both cases, the PSFs and their convolutions with Gaussian-distributed sources are calculated for the optimized slit width of 22 μm for XFD and pinhole sizes of 13 μm for XPC. As shown in Fig. 10, when the source size is 1 μm (r.m.s.), in the XFD, the bottom intensity of the dip rises by 26 % compared to the PSF. On the other hand, in the XPC case, the FWHM width of the convoluted pattern broadens by 8 % compared to the PSF. The rise of the bottom intensity in the XFD with increasing source size is obviously more sensitive than the broadening of the FWHM width in the XPC. Therefore, we can see that XFD has a higher sensitivity to changes in micron-order source sizes than the XPC, and the example of Fig. 10 (a) indicates that XFD can resolve even sub-micron source sizes.

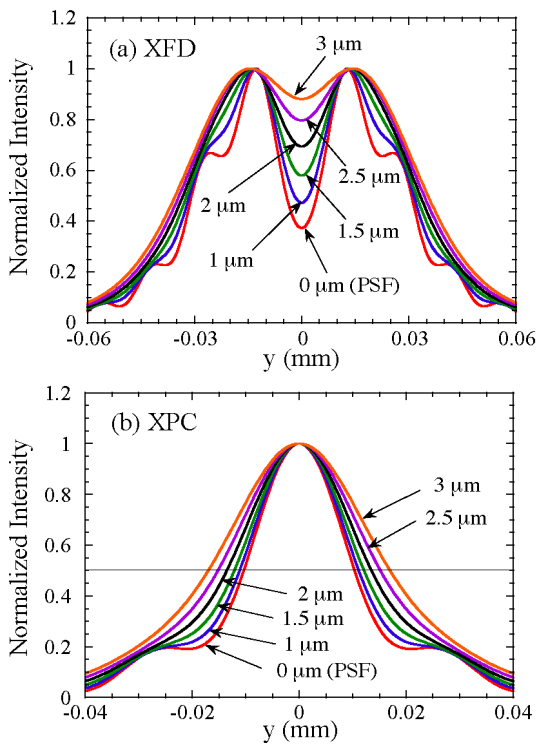

Figure 10: The diffraction patterns for the Gaussian source sizes from zero to 3 μm (r.m.s.). (a) XFD case with a slit width of 22 μm and (b) XPC case with a pinhole size of 13 μm are shown.

CONCLUSION

We have developed a new emittance diagnostics technique, X-ray Fresnel Diffractometry (XFD) to measure micron-order beam size at ID source point. Experimental Study at SPring-8 have shown that XFD is sensitive to micron–order change in the beam size at the ID source point and the light source size smaller than 10 μm (r.m.s.) was successfully resolved with sub-micron resolution. The XFD with an optimized setting has potential to resolve sub-micron beam sizes. This new method is a promising emittance diagnostic technique to maximize the performance of ring-based next-generation light sources.

ACKNOWLEDGMENTS

We would like to thank Dr. T. Watanabe for fruitful discussions and his useful comments, and Nano-forensic Science Group of SPring-8 for their kindness in allowing us to use a high-resolution X-ray imaging system for this experiment.

REFERENCES

[1] R. Hettel and M. Borland, Proceedings of NA-PAC2013, Pasadena, CA, USA, p. 19, (2013).
[2] A. Andersson, *et al.*, Nucl. Instrum. Methods Phys. Res. A, 591, p. 437, (2008).
[3] K.P. Wootton, *et al.*, Phys. Rev. Lett. 109, 194801 (2012).
[4] C. Thomas, *et al.*, Phys. Rev. ST-AB, 13, 022805 (2010).
[5] H. Sakai, *et al.*, Phys. Rev. ST-AB, 10, 042801 (2007).
[6] S. Takano, *et al.*, Nucl. Instrum. Methods Phys. Res. A, 556, p. 357, (2006).
[7] T. Mitsuhashi, *et al.*, Proceedings of DIPAC 2001, Grenoble, France, p. 26 , (2001).
[8] M. Masaki and S. Takano, J. Synchrotron. Rad., 10, p. 295, (2003).
[9] M. Masaki, *et al.*, submitted to Phys. Rev. ST-AB.
[10] S. Takano, *et al.*, Proceedings of IBIC 2012, Tsukuba, Japan, p. 186, (2012).
[11] M. Masaki, *et al.*, Proceedings of SRI 2009, Melbourne, Australia, in AIP Conf. Proc.,Vol.1234, p. 560, (2010).

ISBN 978-3-95450-141-0